





Reproducibility and Radiation Effect of High-Resolution *In Vivo* Micro Computed Tomography Imaging of the Mouse Lumbar Vertebra and Long Bone

HONGBO ZHAO,^{1,2} CHIH-CHIANG CHANG,² YANG LIU,^{2,3} YOUWEN YANG,² WEI-JU TSENG,²
CHANTAL M. DE BAKKER,² REBECCA CHUNG,² PRIYANKA GHOSH,² LINHONG DENG ^{1,4}
and X. SHERRY LIU ²

¹Key Laboratory of Biorheological Science and Technology, Ministry of Education, and Bioengineering College, Chongqing University, Chongqing, China; ²McKay Orthopaedic Research Laboratory, Department of Orthopaedic Surgery, Perelman School of Medicine, University of Pennsylvania, 332A Stemmler Hall, 36th Street and Hamilton Walk, Philadelphia, PA 19104, USA; ³Department of Orthodontics, Stomatological Hospital of Chongqing Medical University, Chongqing, China; and ⁴Changzhou Key Laboratory of Respiratory Medical Engineering, Institute of Biomedical Engineering and Health Sciences, Changzhou University, Changzhou 213164, Jiangsu, China

(Received 6 May 2019; accepted 11 July 2019; published online 29 July 2019)

Associate Editor Michael S. Detamore oversaw the review of this article.

Abstract—A moderate radiation dose, *in vivo* μ CT scanning protocol was developed and validated for long-term monitoring of multiple skeletal sites (femur, tibia, vertebra) in mice. A customized, 3D printed mouse holder was designed and utilized to minimize error associated with animal repositioning, resulting in good to excellent reproducibility in most cortical and trabecular bone microarchitecture and density parameters except for connectivity density. Repeated *in vivo* μ CT scans of mice were performed at the right distal femur and the 4th lumbar vertebra every 3 weeks until euthanized at 9 weeks after the baseline scan. Comparing to the non-radiated counterparts, no radiation effect was found on trabecular bone volume fraction, osteoblast and osteoblast number/surface, or bone formation rate at any skeletal site. However, trabecular number, thickness, and separation, and structure model index were sensitive to ionizing radiation associated with the μ CT scans, resulting in subtle but significant changes over multiple scans. Although the extent of radiation damage on most trabecular bone microarchitecture measures are comparable or far less than the age-related changes during the monitoring period, additional considerations need to be taken to minimize the confounding radiation factors when designing experiments using *in vivo* μ CT imaging for long-term monitoring of mouse bone.

Keywords—*In vivo* μ CT, Bone microarchitecture, Mouse bone, Ionizing radiation.

INTRODUCTION

Micro computed tomography (μ CT) has been widely used to study 3-dimensional (3D) microstructure of bone specimens. In the recent decade, *in vivo* μ CT scanners have also become available to longitudinally monitor skeletal changes in various rodent species.^{2,4-6,17,31} Current *in vivo* μ CT scanners can produce images with an isotropic voxel size on the order of 10 μ m, the resolution of which is high enough for assessment of the 3D cortical and trabecular bone microstructure of small rodents. For accurate measurements of bone microstructure over time, it is critical to understand the reproducibility of these measurements in different scan protocols. Although the reproducibility of *in vivo* μ CT measurements have been reported in rats and mice, the scanning site of these *in vivo* studies have been limited to the proximal tibia, tibial midshaft, and caudal vertebra.^{2,3,10,18,23,28} In addition to the tibia and caudal vertebra, the femur and lumbar vertebra have also been widely used in skeletal research. However, the influence of animal repositioning and motion artifacts associated with *in vivo* scans at these important skeletal sites have not been studied.

Despite the many benefits from longitudinal, *in vivo* μ CT measurements, there are concerns regarding the

Address correspondence to Linhong Deng, Changzhou Key Laboratory of Respiratory Medical Engineering, Institute of Biomedical Engineering and Health Sciences, Changzhou University, Changzhou 213164, Jiangsu, China and X. Sherry Liu, McKay Orthopaedic Research Laboratory, Department of Orthopaedic Surgery, Perelman School of Medicine, University of Pennsylvania, 332A Stemmler Hall, 36th Street and Hamilton Walk, Philadelphia, PA 19104, USA. Electronic mails: dlh@cczu.edu.cn, xiaoweil@pennmedicine.upenn.edu

exposure of tested animals to ionizing radiation. Pre-clinical studies have suggested that focal ionizing radiation damages bone formation by reducing osteoblast number, altering osteoblast differentiation ability, and increasing osteoblast and osteocyte apoptosis.^{11,12,22,30} The effects of radiation on osteoclasts are dose dependent. While 2 Gy whole body radiation increases osteoclast activity,^{16,32} focal radiation with higher dose (2.5–20 Gy) leads to inhibited osteoclast activity.^{7,8,24} Therefore, it is important to understand the radiation effects associated with *in vivo* μ CT when designing an appropriate imaging protocol for the long-term monitoring of multiple skeletal sites (femur, tibia, vertebra) in mice. However, to date, only a limited number of studies have addressed this in mice. Laperre *et al.* tested radiation effects of μ CT protocols with a range of radiation exposures (166–776 mGy) and image voxel sizes on mouse tibiae after 3 repeated scans, with each scan separated by a 2-week interval. While the scanning protocol using a high radiation dose led to significant bone loss in the irradiated tibia, the protocol using a low radiation dose resulted in poor image quality. In contrast, an optimized scanning protocol of moderate exposure to radiation (434 mGy) and 9 μ m nominal voxel size resulted in minor radiation effects and good image quality.¹⁹ Another study by Klinck *et al.* tested radiation effects of a weekly scanning protocol for 3–5 weeks on multiple mouse strains and showed a significant decrease in bone volume fraction (BV/TV) in the irradiated tibiae at 10.5 μ m nominal voxel size.¹⁴ Furthermore, Willie *et al.* reported significantly lower BV/TV in the tibiae of 10-week-old mice after exposure to 4 repeated scans (5-day interval) at 10.5 μ m nominal voxel size when compared to those only exposed to a single scan.³³ In contrast, no radiation effect was found in 26-week-old mice based on the same experiment protocol. Additionally, it was reported by Schulte *et al.* that no radiation effect was observed on the 6th caudal vertebra of mouse after 5 weekly scans at 10.5 μ m nominal voxel size.²⁷

All of these studies suggest that different scan settings, such as image voxel size and scan frequency, may have differing effects on bone. Moreover, skeletal sites and animal age may also affect the response to the radiation exposure associated with *in vivo* μ CT scans. The previous studies focused on the radiation effect over a relative short monitoring period (4–5 weeks). In order to enable longer monitoring for mouse bone changes, we designed an imaging strategy to monitor the mouse femur at 10.5 μ m and lumbar vertebra at 15 μ m nominal voxel size every 3 weeks for a 9-week period. Taking into account these important findings from previous investigations, the purpose of this study was to establish a moderate-dose, *in vivo* μ CT scanning protocol and measurement regimen that yields the

necessary precision to monitor changes in adult mouse vertebrae and long bones and to investigate the radiation effects of this protocol on bone quality and bone cell activities.

In the current study, the first objective was to examine the short-term reproducibility of mouse trabecular bone microstructure measurements at the distal femur and lumbar vertebra and cortical measurements at the tibial midshaft when utilizing customized scan holders. The second objective was to test whether a 3D image registration technique can reduce the precision error caused by repositioning of the animals. Lastly, the third objective of this study was to examine the radiation effect at both the tissue and cellular level when using this newly developed *in vivo* μ CT scanning protocol. We hypothesized that a well-designed *in vivo* μ CT scan and analysis protocol can maximize the reproducibility in mouse vertebral and long bone microstructural measurements between multiple scans with minimized radiation effects.

MATERIALS AND METHODS

Animal Protocol

All animal procedures were reviewed and approved by the University of Pennsylvania's Institutional Animal Care and Use Committee. Twenty-five female C57BL/6J (BL6) mice were purchased (age 11–12 weeks old) from The Jackson Laboratory (Bar Harbor, ME). Ten mice were used to assess the reproducibility of the *in vivo* μ CT scanning protocol. These mice underwent multiple scans within a 24-h period and were euthanized following the last scan. To assess radiation effects of *in vivo* μ CT scans, eight mice were subjected to *in vivo* scans every 3 weeks and euthanized 9 weeks after the first scan to evaluate the radiation effect incurred. Additionally, 7 mice underwent *in vivo* scans at the age of 12 and 21 weeks to assess age-related changes in bone.

In Vivo μ CT Scans to Assess Imaging Reproducibility

A total of 4 sets of scans were performed for each mouse. Each set consists of scans of the 4th lumbar vertebra (L4), right distal femur, and right tibial midshaft, for a total of 30 min. Between each set of scans, the mouse was removed from the holder and allowed to recover from anesthesia, with ample heat to regulate body temperature and full access to food and water for at least 2 h. The 4 sets of scans were completed within a 24-hour period.

Mice were anesthetized in an induction chamber using isoflurane (4%) dissolved in oxygen and then transferred to a nose cone and placed on the scanning

bed. The anesthesia was maintained (2.25% delivery rate) for the duration of the scanning period. All mice were scanned by an *in vivo* μ CT system (Scanco vivaCT40, Scanco Medical AG, Brüttisellen, Switzerland). An animal holder fixture was custom-designed using SolidWorks software (Dassault Systèmes, Vélizy-Villacoublay, France) and fabricated using a 3D printer (Makerbot Replicator 2X, Stratasys Ltd, Eden Prairie, MN). The design principle, fabrication, and operation protocol for the mouse holder fixture is provided in the Supplemental Material with an input file (in.stl format) for 3D printing to download. The customized animal holder fixture served to minimize motion artifact and ensure that scan sites were positioned in a similar 3D orientation between scans. The animal holder fixture consists of three major parts. Two disks were designed to connect to the scanner-provided long bed and also prevent the soft tissue from crossing the border of the focus region of the x-ray tube. The bed between the two disks maintained the mice within the focusing region for the vertebra scan. A small u-shaped component further immobilized the femur (Fig. 1). Before each scan, the mouse body was stretched out and laid in a supine position on the holder, and carefully restrained using Coban self-adherent wrap (3M, St. Paul, MN) to minimize motion without blocking blood flow and hindering breathing. A 2D scout view image (Fig. 1) was used to determine the region of interest. The highest achievable scan resolution is inversely associated with the smallest diameter of the cross-sectional field of view (FOV) that the scanned object can fit within. Based on the average dimensions of the mouse hind limb and abdominal region, highest nominal voxel size for scans of the distal femur and lumbar vertebra was determined to be $10.5\ \mu\text{m}$ and $15\ \mu\text{m}$, respectively. For the distal femur, a 2.2 mm region consisting of 208 slices immediately proximal to the growth plate were scanned at $10.5\ \mu\text{m}$ nominal voxel size. For the L4, a 3.1 mm region consisting of 209 slices at the center of the vertebral body were scanned at $15\ \mu\text{m}$ nominal voxel size. For the tibial midshaft, a 2.2 mm region consisting of 208 slices at the center of the tibia were scanned at $10.5\ \mu\text{m}$ nominal voxel size. The scanner was operated at 55 kVp energy, $145\ \mu\text{A}$ intensity, and 200 ms integration time, and the average time for scan at each skeletal site was approximately 10 min.

Image Registration and Microstructural Analysis of Trabecular Bone

To register the baseline (I_1) and three follow-up scans (I_2 , I_3 , and I_4), we used a landmark-initialized, mutual information based image registration software

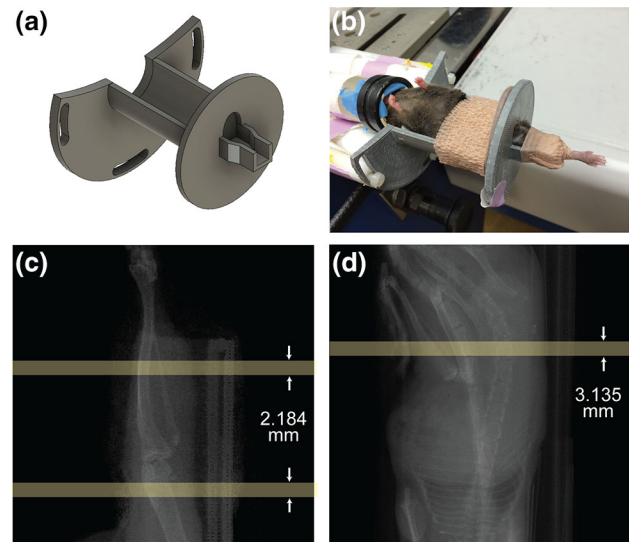


FIGURE 1. (a) Customized jig for holding the mouse tibia to ensure minimal motion artifacts and similar positions over longitudinal scans. (b) *In vivo* μ CT scan of a mouse under anesthesia with the right tibia held by customized jig. (c, d) Scout view of (c) tibia and femur and (d) lumbar spine for selection of the region of interest for scans. The regions for scans are highlighted in yellow.

(National Library of Medicine Insight Segmentation and Registration Toolkit).^{9,25} Detailed information regarding the registration approach can be found in the ITK Software Guide^{25,26} and in our previous studies.^{1,18}

For trabecular bone analysis, the strategy entailed identifying the common volume of interest (VOI) within trabecular bone compartments of the baseline and follow-up scans without rotating the scanned images to avoid interpolation error, as illustrated in Fig. 2.^{1,18} Briefly, for each mouse, the last follow-up scan (I_4) was registered to each of the previous scans (I_1 , I_2 , and I_3), resulting in a set of transformation matrices that represent the rigid-body transformations, including 3D rotations and translations, between image coordinates of the three scan pairs. To obtain a common VOI of trabecular bone in all four scans, the trabecular bone compartment of I_4 was semi-automatically contoured and saved as a VOI mask (gobj file, V_4). For the distal femur, the VOI included a 1.0 mm segment of trabecular bone, beginning 0.1 mm to 1.1 mm proximal to the growth plate. For the L4, VOI included a 1.8 mm segment in the center of the vertebra. Then, the transformation matrices between I_4 and each of the I_1 , I_2 , and I_3 were applied to rotate and translate the VOI mask V_4 to new VOI masks (V_1 , V_2 , and V_3). The new VOI masks (V_1 , V_2 , and V_3 , gobj files) identified the VOIs in the scans I_1 , I_2 , and I_3 that corresponded to the same VOI of the scan I_4 . A

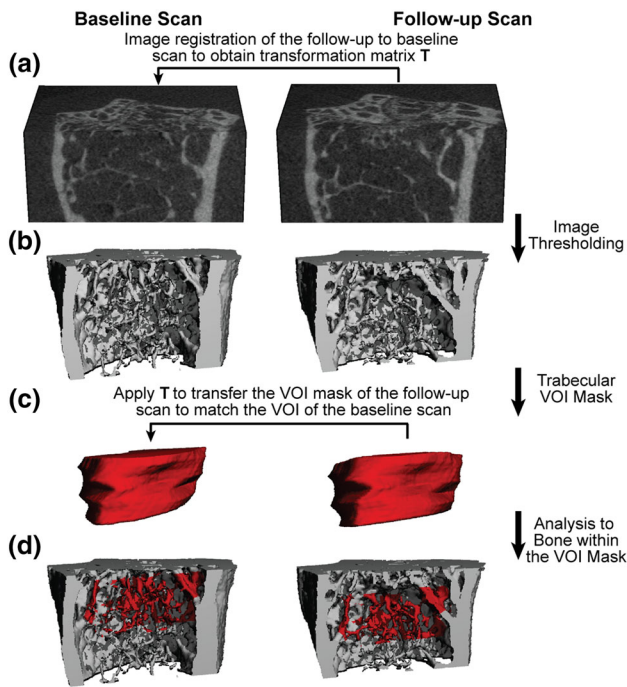


FIGURE 2. Schematics of the image registration for trabecular bone analysis: (a) Image registration was performed on greyscale images to obtain the translation matrix T . (b) Image thresholding was performed to distinguish bone matrix from bone marrow and background. (c) A trabecular VOI mask was generated based on the thresholded follow-up scan to separate trabecular from cortical compartment. Then the transformation matrix T was applied to transform the VOI mask of the follow-up scan to the corresponding VOI of the baseline scan. (d) Trabecular microstructural analysis was then performed on the trabecular bone within the corresponding VOIs (highlighted red region) of both baseline and follow-up scans.

manual check was performed to ensure that the registered VOIs were within the scanned region in all scans (I_1 – I_4). Subsequently, the registered, thresholded trabecular VOIs in all scans were subjected to microstructural analysis.

All trabecular bone images were smoothed using a Gaussian filter ($\sigma = 0.6$, $\text{support} = 1$), followed by a segmentation threshold corresponding to 450.7 mgHA/cm^3 . Bone volume fraction (BV/TV), trabecular number (Tb.N), trabecular thickness (Tb.Th), trabecular separation (Tb.Sp), connectivity density (Conn.D), structure model index (SMI), volumetric bone mineral density (Tb.vBMD), and tissue mineral density (Tb.TMD) were calculated by 3D standard microstructural analysis software provided by the manufacturer.

For the unregistered images, a 1.0 mm region of femoral trabecular bone, beginning 0.1–1.1 mm proximal to the growth plate and a 1.8 mm region at the center of the vertebra were contoured and analyzed for the baseline and follow-up bone scans.

Image Registration and Microstructural Analysis of Cortical Bone

The strategy used in trabecular bone analysis, *i.e.*, identification of the common VOIs of cortical bone, would not allow assessment of variability in cortical morphology between different scans, as the VOI is defined as the precise cortical geometry for an image, which may not translate to the cortical geometry at other time points. Therefore, a different image transformation approach was used to assess the cortical bone structure of the registered μCT images of the tibial midshaft. Briefly, each of the follow-up scans (I_2 , I_3 , and I_4) was registered to the baseline scan I_1 . The resulting transformation matrices were applied to rotate and translate the greyscale image of each of the I_2 , I_3 , and I_4 so that the coordinates of the transformed images (I_2' , I_3' , and I_4') aligned with those of I_1 . Then, a 0.8 mm segment of cortical bone, corresponding to 80 slices located at the center of the tibia, was semi-automatically contoured for I_1 . Subsequently, the cortical bone of the transformed follow-up images I_2' , I_3' , and I_4' were semi-automatically contoured for 80 slices, corresponding to the same location of I_1 .

All cortical bone images were smoothed by application of a Gaussian filter ($\sigma = 1.2$, $\text{support} = 2$) and a global threshold corresponding to 628.6 mgHA/cm^3 . Cortical bone parameters, including cortical area (Ct.Area), cortical thickness (Ct.Th), polar moment of inertia (pMOI), tissue mineral density (TMD), and cortical porosity (Ct.Po) were measured.

For the unregistered images of tibial midshaft, 80 slices located at the center of the tibia were contoured and analyzed for the baseline and follow-up bone scans.

In Vivo and Ex Vivo μCT Scans to Evaluate Radiation Effect

Eight mice received a baseline scan at the right distal femur and the L4, follow-up scans every 3 weeks and were killed at 9 weeks after the initial baseline scan. The *in vivo* μCT scans followed the same protocol described in the Sect. 2.2 with a $10.5 \mu\text{m}$ nominal voxel size at the right distal femur and $15 \mu\text{m}$ nominal voxel size at the L4. Radiation dose was calculated using an ionizing chamber (DCT10-RS, IBA Dosimetry GmbH, Schwarzenbruck, Germany) that was attached to a measurement unit (Solidose 400, RTI Group, Mölnådal, Sweden) in the center of a 35 mm polymethyl methacrylate (PMMA) tube. This scanning protocol induced a radiation dose of 639 mGy for scans of the femur and 310 mGy for scans of the vertebra. Anti-scatter collimators were placed by the manufacturer in front of detectors to minimize stray radiation outside

the scanned area. Outside the FOV, direct radiation may affect up to 150 μ m in the axial direction. Further away, the amount of stray radiation is primarily due to scattering from the animal tissue within the FOV, and thus is negligible compared to that inside the FOV. Therefore, the unscanned left femur and L3 vertebra (~ 0.5 mm from the L4) were used as non-radiated controls.

Following euthanasia of the mice, the left and right femurs, and L3 and L4 vertebrae were harvested and underwent *ex vivo* scans at a 6 μ m nominal voxel size using a μ CT scanner (MicroCT35, Scanco Medical AG, Brüttisellen, Switzerland). For the distal femur, a 0.9 mm segment in the secondary spongiosa right below the growth plate, corresponding to 150 image slices, was subjected to analysis. For the L3 and L4, a 1.4 mm segment in the center of the vertebra, corresponding to 227 image slices, was subjected to the same analysis protocol previously described in Sect. 2.3.

Static and Dynamic Histomorphometry

All mice received subcutaneous injections of calcein (15 mg/kg, Sigma-Aldrich, St. Louis, MO) at 9 and 2 days prior to euthanasia, and the left and right femurs, and L3, and L4 vertebrae were processed for undecalcified histology after *ex vivo* μ CT scans. Specimens were embedded in methyl methacrylate (MMA), sectioned using a Polycut-S motorized microtome (Reichert, Heidelberg, Germany), and then subjected to static and dynamic bone histomorphometric analysis. For static bone histomorphometry, 5 μ m-thick sections were cut (Polycut-S motorized microtome, Reichert) and subsequently stained with Goldner's trichrome, and osteoblast number (Ob.N/BS), osteoclast number (Oc.N/BS), osteoblast surface (Ob.S/BS) and osteoclast surface (Oc.S/BS) were measured in the region scanned by *in vivo* μ CT. For dynamic bone histomorphometry, 8 μ m-thick sections were cut (Polycut-S motorized microtome, Reichert). Based on the calcein labeling, measurements of bone formation rate (BFR/BS), mineral apposition rate (MAR), and mineralizing surfaces (MS/BS) were quantified at the same location where static bone histomorphometry

Osteo Software (Bioquant Image Analysis, Nashville, TN).

Evaluation of Age-Related Changes in Bone

Seven mice underwent *in vivo* μ CT scans at the right distal femur and the L4 at the age of 12 and 21 weeks to assess age-related changes in bone. The *in vivo* μ CT scans, image processing, and bone microstructure analysis followed the same protocols as previously described in Sects. 2.2 and 2.3. Percent changes of bone microstructure parameters over 9 weeks of aging were also calculated.

Statistical Analysis

All results are presented as mean \pm standard deviation (SD). To evaluate the reproducibility of each measurement, the individual coefficient of variance (CV) was calculated, and the root mean square average of the %CV (RMSCV) was derived for both the unregistered and registered image pairs.

For each image pair i , $i = 1, 2, \dots, N$, ($N = 10$)

$$\%CV_i = \frac{SD_i}{\text{Mean}_i} \times 100\%$$

$$\text{RMS}_{\%CV} = \sqrt{\sum_{i=1}^N \%CV_i^2 / N}$$

$$\text{RMS}_{SD} = \sqrt{\sum_{i=1}^N SD_i^2 / N}$$

Intraclass correlation coefficient (ICC), as previously described in ²⁹ and ¹⁵ is defined as the ratio of the variance due to differences amongst samples to the total population variance. The total variability encompasses inherent differences amongst samples as well as the differences caused by the measurement technique used during the repetitive measurements. ICC varies between 0 and 1, where an ICC close to 1 indicates good test-retest repeatability. ICCs were calculated based on the mean squares determined through a two-way ANOVA, as follows ^{15,29}:

$$\text{ICC} = \frac{\text{MS}_{\text{between}} - \text{MS}_E}{\text{MS}_{\text{between}} + (N_{\text{measures}} - 1) \times \text{MS}_E + N_{\text{measures}} \times (\text{MS}_{\text{within}} - \text{MS}_E) / N_{\text{samples}}}$$

was performed. All static and dynamic histomorphometry measurements were made using Bioquant

where $\text{MS}_{\text{between}}$ is between-samples mean square, $\text{MS}_{\text{within}}$ is within-samples mean square (i.e., between-

measurements mean square), MS_E is error mean square, $N_{measures}$ is number of repeated measures = 4, $N_{samples}$ is number of samples = 10.

Paired Student's *t*-tests were performed to compare the %CV of repeated scans before and after image registration and to compare the radiated and non-radiated microstructure and cellular activities in bone. Two-sided *p*-values less than 0.05 were considered significant.

RESULTS

Reproducibility of In Vivo μ CT Measurements of Femoral Trabecular Bone

Prior to image registration, the precision errors ($RMS_{\%CV}$) associated with BV/TV, Tb.N, Tb.Th, Tb.Sp, SMI, Tb.BMD, and Tb.TMD of the distal femur ranged between 0.605% and 5.80% (Table 1). The precision error was particularly high for Conn.D (13.4%). After image registration, on average, preci-

sion errors of all measurements but Conn.D decreased to levels below 2%, ranging between 0.502 and 1.97%. A trend of improvement in Conn.D was achieved by image registration ($p = 0.09$), resulting in a moderate reproducibility for Conn.D at 8.17%. Moreover, improvement in precisions of BV/TV, Tb.N, Tb.Th, Tb.Sp, SMI, and Tb.BMD reached statistical significance (Table 1). Prior to registration, ICCs ranged from 0.789 to 0.939. After registration, ICCs for microstructure parameters (BV/TV, Tb.N, Tb.Th, Tb.Sp, SMI, and Conn.D) ranged from 0.952 to 0.986 and for density measurements were 0.981 (Tb.BMD) and 0.882 (Tb.TMD).

Reproducibility of In Vivo μ CT Measurements of Vertebral Trabecular Bone

Similar results were found for vertebral bone. Prior to image registration, most parameters can be reproduced with less than 5% precision errors with exceptions for Conn.D (8.94%) and SMI (6.09%, Table 2).

TABLE 1. Reproducibility parameters for the femur: mean, standard deviation (SD), and coefficient of variance (CV = SD/mean) of baseline measures, root mean square of standard deviation (RMS_{SD}), and root mean square of percent coefficient of variance ($RMS_{\%CV}$) of repeated trabecular bone measurements of the distal femur based on registered and unregistered scans.

Distal Femur	BV/TV	Tb.N(1/mm)	Tb.Th(mm)	Tb.Sp(mm)	Conn.D(1/mm ³)	SMI	Tb.TMD(mg Hg/cm ³)
Bone measurements							
Mean \pm SD	0.103 \pm 0.018	4.88 \pm 0.46	0.0396 \pm 0.0014	0.206 \pm 0.018	138 \pm 51	2.63 \pm 0.22	857 \pm 10
CV	0.174	0.095	0.036	0.089	0.369	0.083	0.012
Reproducibility based on unregistered scans							
RMS_{SD}	0.00665	0.117	0.000476	0.00466	19.6	0.0717	5.20
$RMS_{\%CV}$	5.80%	2.36%	1.20%	2.29%	13.4%	2.94%	0.605%
ICC	0.876	0.939	0.895	0.937	0.867	0.900	0.789
Reproducibility based on registered scans							
RMS_{SD}	0.00228*	0.0557*	0.000287*	0.00247*	9.10	0.0271*	4.31
$RMS_{\%CV}$	1.97%*	1.13%*	0.730%*	1.20%*	8.17%	1.10%*	0.502%
ICC	0.984	0.983	0.952	0.980	0.970	0.986	0.882

Significant improvement in SD and %CV from the unregistered comparison was indicated by * $p < 0.05$.

TABLE 2. Reproducibility parameters for the L4: mean, standard deviation (SD), and coefficient of variance (CV = SD/Mean) of baseline measures, root mean square of standard deviation (RMS_{SD}), and root mean square of percent coefficient of variance ($RMS_{\%CV}$) of repeated trabecular bone measurements of the L4 based on registered and unregistered scans.

L4	BV/TV	Tb.N(1/mm)	Tb.Th(mm)	Tb.Sp(mm)	Conn.D(1/mm ³)	SMI	Tb.TMD(mg Hg/cm ³)
Bone measurements							
Mean \pm SD	0.189 \pm 0.037	4.97 \pm 0.61	0.048 \pm 0.003	0.206 \pm 0.025	237 \pm 54	1.96 \pm 0.44	755 \pm 18
CV	0.195	0.123	0.068	0.121	0.228	0.224	0.023
Reproducibility based on unregistered scans							
RMS_{SD}	0.00753	0.0759	0.000730	0.00354	18.9	0.129	10.4
$RMS_{\%CV}$	4.68%	1.64%	1.48%	1.56%	8.94%	6.09%	1.41%
ICC	0.960	0.985	0.953	0.980	0.888	0.919	0.728
Reproducibility based on registered scans							
RMS_{SD}	0.00487*	0.0551	0.000753	0.002819	14.1	0.089*	8.55
$RMS_{\%CV}$	2.98%*	1.18%	1.58%	1.28%	7.14%	4.16%*	1.15%
ICC	0.983	0.991	0.954	0.986	0.923	0.964	0.753

Significant improvement in SD and %CV from the unregistered comparison was indicated by * $p < 0.05$.

TABLE 3. Reproducibility parameters for the tibial midshaft: mean, standard deviation (SD), and coefficient of variance (CV = SD/ Mean) of baseline measures, root mean square of standard deviation (RMS_{SD}), and root mean square of percent coefficient of variance (RMS_{%CV}) of repeated cortical bone measurements of the tibial midshaft based on registered and unregistered scans.

Tibia midshaft	Ct.Area (mm ²)	Ct.Th (mm)	pMOI (mm ⁴)	Ct.Po (%)	Ct.TMD(mg Hg/cm ³)
Bone measurements					
Mean \pm SD	0.483 \pm 0.030	0.165 \pm 0.008	0.102 \pm 0.013	0.115 \pm 0.005	1133 \pm 19
CV	0.063	0.048	0.129	0.048	0.017
Reproducibility based on unregistered scans					
RMS _{SD}	0.00642	0.00186	0.00363	0.00166	5.95
RMS _{%CV}	1.37%	1.11%	3.59%	1.45%	0.529%
ICC	0.957	0.948	0.928	0.913	0.910
Reproducibility based on registered scans					
RMS _{SD}	0.00337*	0.00114	0.00169*	0.00246	5.66
RMS _{%CV}	0.689%*	0.686%	1.88%*	2.07%	0.502%
ICC	0.989	0.984	0.987	0.828	0.915

Significant improvement in %CV from the unregistered comparison was indicated by * $p < 0.05$.

After image registration, precision errors of BV/TV, Tb.N, Tb.Th, Tb.Sp, Tb.BMD, and Tb.TMD were reduced to levels below 3% and below 4.16% for SMI. Particularly, precisions of BV/TV and SMI were significantly improved. However, only a moderate reproducibility was achieved for Conn.D after image registration (7.14%). Prior to registration, ICCs ranged from 0.728 to 0.985. After registration, ICCs for microstructure parameters (BV/TV, Tb.N, Tb.Th, Tb.Sp, SMI, and Conn.D) ranged from 0.923 to 0.991 and for density measurements were 0.979 (Tb.BMD) and 0.753 (Tb.TMD).

Reproducibility of In Vivo μ CT Measurements of the Tibial Midshaft

Precision errors associated with cortical bone parameters at the tibial midshaft ranged from 0.529 to 3.59% prior to image registration, and from 0.502 to 1.88% after image registration (Table 3). Reproducibility of Ct.Area and pMOI were significantly improved by image registration. In contrast, the average precision error of Ct.Po increased from 1.45 to 2.07% after image registration. Image registration resulted in higher values of ICCs for Ct.Area, Ct.Th, pMOI, and Ct.TMD, ranging from 0.915 to 0.989. However, ICC for Ct.Po decreased from 0.913 to 0.828 after image registration.

Radiation Effect on the Distal Femur

Comparisons between non-radiated left femur and radiated right femur showed no difference in BV/TV, Conn.D, and TMD. However, the radiated right femur had 5.5% lower Tb.N and 13.8%, 14.7%, and 7.0% greater SMI, Tb.Th, and Tb.Sp, respectively, than the non-radiated left femur (Fig. 3). No difference was found in any measurement of bone cell numbers, sur-

faces, or formation activities between the non-radiated and radiated femurs (Fig. 3).

Radiation Effect on the Lumbar Vertebra

Comparisons between non-radiated L3 and radiated L4 suggested no difference in most of trabecular bone microstructure parameters with the exception of Tb.N and Tb.Sp. Radiated L3 had 9.6% lower Tb.N and 12.1% greater Tb.Sp than non-radiated L4 (Fig. 4). No difference was found in any measurement of bone cell numbers, surfaces, or formation activities between the non-radiated and radiated femurs (Fig. 4).

Age-Related Changes of the Distal Femur and Lumbar Vertebra

Comparisons between the baseline and endpoint scans suggested a 55% loss in BV/TV in the distal femur from the age of 12 to 21 weeks, which was associated with a 31% and 71% reduction in Tb.N and Conn.D, and 47% increase in Tb.Sp, respectively (Table 4). No reduction in BV/TV was found for the L4 over the course of 9 weeks. However, Tb.N decreased by 11% and Tb.Sp increased by 14%.

DISCUSSION

In this study, we developed and validated a moderate-dose, *in vivo* μ CT scan protocol which can be applied to scan multiple skeletal sites (femur, tibia, vertebra) in mice. By utilizing a custom-designed holder and well-established image registration techniques, excellent reproducibility was achieved for all skeletal sites. At the highest *in vivo* μ CT image resolution (nominal image voxel size of 10.5 μ m and 15 μ m for the femur and vertebra, respectively), radiation

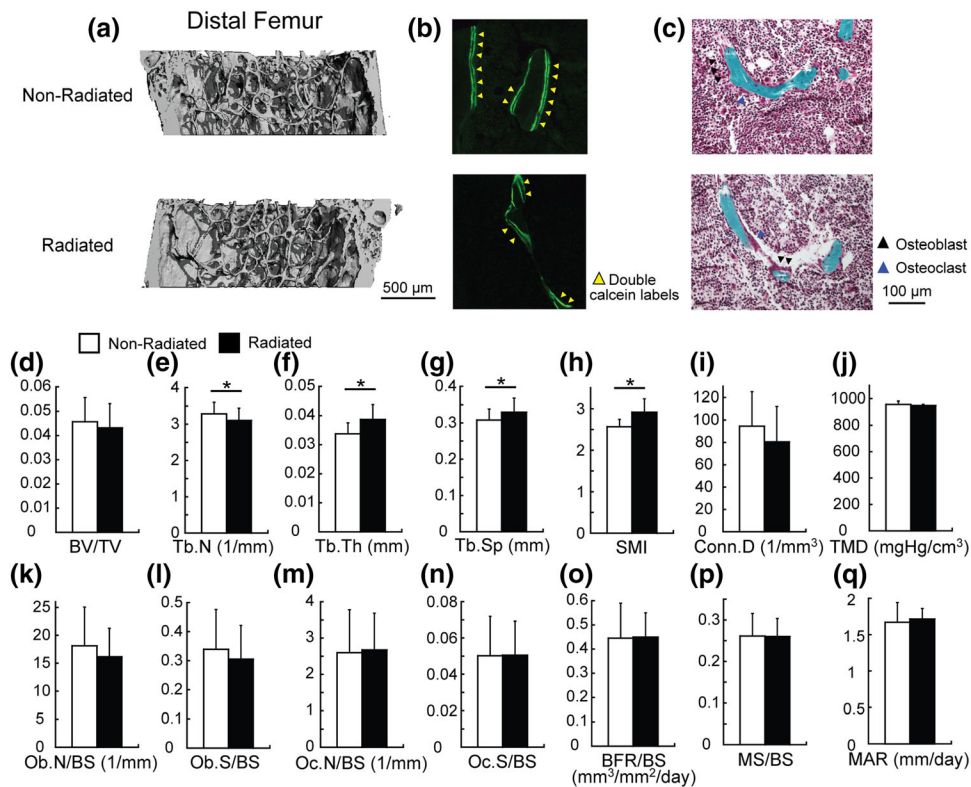


FIGURE 3. Representative images of (a) 3D rendering of distal femoral bone, (b) calcein-labeled bone surfaces with yellow arrow indicating double-labeled surfaces, and (c) bone histomorphometry with black arrow indicating osteoblasts and blue arrow indicating osteoclasts on the bone surface in the (Top) non-radiated and (Bottom) radiated femur. (d–j) Comparisons in trabecular bone microstructural and density parameters between the non-radiated and radiated femurs. (k–q) Comparisons in the static and dynamic bone histomorphometry parameters between the non-radiated and radiated femurs.

exposure due to repeated, *in vivo* μ CT scans resulted in small but significant changes in some of the bone microstructure parameters while bone volume fraction, number, and surface of osteoblasts and osteoclasts were not affected.

The reproducibility of bone density and microstructure measurement by *in vivo* μ CT imaging has previously only been evaluated for the mouse tibia.^{20,21,23} The current protocol overcomes this limitation by enabling multiple skeletal sites in mice to be scanned. According to our results, reasonable precision ($\text{RMS}_{\%CV}$) can be achieved via use of our customized holder along with the standard microCT scan and analysis at all three skeletal sites for most microstructure and density measurements with the exception of Conn.D.

At the distal femur, 3D image registration resulted in significant improvements in precision for most bone microstructure parameters. This differs from results reported by Nishiyama *et al.*²³ where no difference was observed between precision errors with and without image registration for the mouse proximal tibia. This may be due to a greater angle between femur alignment and the axial direction of the holder as compared to

the tibia (Fig. 1), which may cause a greater repositioning error associated with femur scans. Nevertheless, the registered precision of most trabecular bone measurements at the distal femur was within 2%, a similar level compared to that reported at the proximal tibia.²³ At the L4, image registration only led to improvement in the precision of BV/TV and SMI, suggesting that minimal repositioning error was associated with the scanning of the lumbar vertebra. For both the femur and L4, the Conn.D measurement had a higher precision error compared to other parameters with and without image registration. The elevated precision error in Conn.D has also been reported in previous studies of rat and mouse,^{15,18,23} which suggests that Conn.D measurements are more sensitive to image quality and motion artifact compared to other microstructure measurements. Furthermore, the mouse strain used in the current study has a low trabecular bone phenotype with a particularly low Conn.D, which also contributed to higher variance in its measurement. Image registration also led to increased ICC in all measurements at the femur and L4. ICCs of most measurements except for Tb.TMD were greater than 0.92, a level greater than those

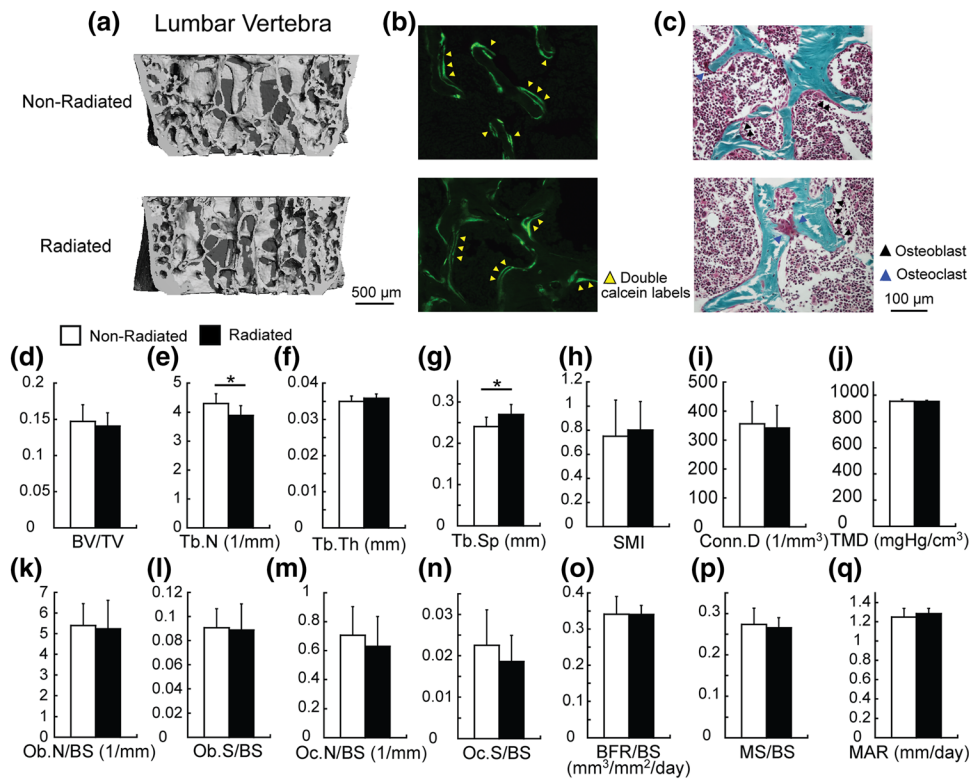


FIGURE 4. Representative images of (a) 3D rendering of vertebral bone, (b) calcein-labeled bone surfaces with yellow arrow indicating double-labeled surfaces, and (c) bone histomorphometry with black arrow indicating osteoblasts and blue arrow indicating osteoclasts on the bone surface in the (Top) non-radiated and (Bottom) radiated lumbar vertebrae. (d–j) Comparisons in trabecular bone microstructural and density parameters between the non-radiated and radiated vertebrae. (k–q) Comparisons in the static and dynamic bone histomorphometry parameters between the non-radiated and radiated lumbar vertebrae.

TABLE 4. Percent change in trabecular bone microstructure at the distal femur and L4 from the age of 12 to 21 weeks.

% change over 9 weeks	BV/TV	Tb.N	Tb.Th	Tb.Sp	Conn.D	SMI	Tb.TMD
Distal Femur	- 52.5 ± 23.9%*	- 29.5 ± 6.1%*	- 2.7 ± 9.2%	43.8 ± 12.7%*	- 70.4 ± 37.4%*	19.2 ± 22.7%	0.1 ± 3.2%
L4	- 5.7 ± 9.0%	- 10.7 ± 7.1%*	3.1 ± 4.3%	14.1 ± 7.9%*	0.6 ± 13.1%	0.7 ± 13.6	- 0.8 ± 2.8

*Indicates significant change ($p < 0.05$).

reported for the proximal tibia.²³ The inherent variation among animals in Tb.TMD is much lower than those of other measurements as reflected by 3-30 times lower coefficient of variance of Tb.TMD than other measurements at the femur and L4 (Table 1 and 2). Therefore, the resulting ICC in Tb.TMD would be lower than other measurements even with similar level of variability among the repeated measurements.

Excellent precision was also found in cortical bone measurements at the tibial midshaft by standard scan and analysis protocol. Image registration further improved precision for Ct.Area and pMOI measurements. However, both precision and ICC decreased after image registration for measurement of Ct.Po. The image processing for registered trabecular bone and

cortical bone analysis are fundamentally different. The trabecular bone analysis only involves identification of the same VOI between baseline and follow-up scans while the cortical bone analysis requires translation, rotation, and image interpolation of the follow-scans in order to match the baseline scan. Due to the partial volume effect that is involved with image rotation and interpolation, measurements such as Ct.Po would be significantly affected, resulting in even lower reproducibility after image registration. Therefore, it is recommended that evaluation of Ct.Po should follow a standard scanning and analysis protocol, without image registration.

Repeated radiation exposure to weekly *in vivo* μ CT scans has been reported to cause significant bone

deterioration in mice.¹⁴ To enable a long-term monitoring of bone changes, the interval between repeated scans was adjusted to 3 weeks in our protocol and the cumulative effect of multiple exposures to scan-induced radiation in a span of 9 weeks was evaluated. At the distal femur, despite no radiation effect on BV/TV, the irradiated femur had reduced number and increased thickness of trabeculae, increased separation between trabeculae, and a more rod-like trabecular network compared to the non-irradiated contralateral femur. At the lumbar vertebra, despite the 50% lower radiation dose compared to the femur, radiated L4 had significantly lower number and increased separation of trabeculae than that of the non-irradiated L3. The radiation dose at L4 (310 mGy) is lower than that of the protocol used for the proximal tibia (434 mGy) in a previously published study by Laperre *et al.*¹⁹ where no radiation effect was reported for any of the trabecular bone microarchitecture parameters. It is possible that the lumbar vertebra is more sensitive to radiation exposure than the proximal tibia. Furthermore, the sample size in the current study is twice than that of the study by Laperre *et al.*¹⁹ thereby allowing the detection of subtle but significant effects of radiation exposure on bone parameters. Surprisingly, we did not observe significant effects of radiation on osteoblast and osteoclast number, surface, nor on the bone formation rate. It is likely that there was an acute response elicited by the bone cells to the ionizing radiation by *in vivo* μ CT, which was not maintained long-term.

Aging also plays a significant role in trabecular bone loss. Results from our study are consistent with those reported by Glatt *et al.*, which showed that female mice had significant bone loss in the distal femur and vertebra from age of 3 to 5 months.¹³ For the distal femur, the extent of radiation damage of Tb.N, Tb.Sp, and SMI (5.5–14.7%) over 9 weeks was far below the mean of age-related bone changes (19.2–70.4%) over the same period of time as well as below the standard deviation (6.1–22.7%). Therefore, the ionizing radiation associated with *in vivo* μ CT exerted significant but negligible effects on these trabecular parameters at the distal femur. Nevertheless, radiation led to a significant increase in Tb.Th while aging exerted no effect. For the lumbar vertebra, aging only caused moderate changes in number and separation of trabeculae without affecting bone mass. Interestingly, exposure to the radiation by *in vivo* μ CT leads to a similar degree of changes in the same trabecular bone microarchitecture parameters without effect on others. Caution needs to be taken when interpreting data acquired by *in vivo* μ CT regarding changes in trabecular microarchitecture, especially for Tb.N and Tb.Sp at the lumbar vertebra as well as Tb.Th at the distal femur. Overall,

the effect of *in vivo* μ CT-associated radiation is relatively subtle compared to aging effect, however one should bear in mind that the confounding radiation factors may be significantly greater compared to intrinsic variation of other diseases or treatment models. Therefore, it is recommended to always include a control group of animals that are subjected to the same frequency and dosage of exposure to *in vivo* μ CT as other experimental groups.

To our knowledge, this is the first study examining the reproducibility and radiation effects of a moderate dose, high-resolution *in vivo* μ CT imaging protocol for both mouse vertebra and long bone. However, our study was limited to female, healthy adult C57BL/6J mice. Although we do not expect the sex, age, or strain would cause significant changes to the precision error associated with our scan protocol, it is possible that mice of different sex, age, or strain are more or less susceptible to radiation-induced changes in bone quality and bone cell activities. To assess the consequence of exposure to radiation, the contralateral femur and adjacent lumbar vertebra were used as non-irradiated counterparts to the radiated bone sites. The limitations of this experiment design include intrinsic differences between the radiated and non-irradiated counterparts and the exposure to stray radiation in these counterparts. Nevertheless, selecting a counterpart within the same test subject increases the statistical power and sensitivity to detect any radiation effect. Moreover, the amount of stray radiation subjected to the unscanned counterparts is negligible compared to the scanned sites due to the built-in anti-scatter collimator by the manufacturer.

In spite of the limitations listed above, this study thoroughly evaluated an *in vivo* μ CT imaging protocol for long-term monitoring of skeletal changes in response to diseases or therapies in a mouse model. The assessment of imaging reproducibility was performed in live animals and the precision error with and without 3D image registration was investigated. A customized, 3D printed mouse holder fixture was designed to reduce precision error, thereby resulting in good to excellent reproducibility in most cortical and trabecular bone parameters, even without image registration. No radiation effects were found in trabecular bone mass and bone cellular activities at both the mouse long bone and lumbar vertebra after a 9-week monitoring period with *in vivo* μ CT scans every 3 weeks. However, it should be noted that trabecular bone microarchitecture parameters are sensitive to the μ CT-induced radiation, resulting in subtle but significant changes over multiple scans. Additional considerations, such as including a control group, need to be taken to minimize the confounding radiation factors

when designing experiments using *in vivo* μ CT imaging to monitor changes in mouse bone.

ELECTRONIC SUPPLEMENTARY MATERIAL

The online version of this article (<https://doi.org/10.1007/s10439-019-02323-z>) contains supplementary material, which is available to authorized users.

ACKNOWLEDGEMENTS

Research reported in this publication was supported by the Penn Center for Musculoskeletal Diseases (PCMD) NIH/NIAMS P30-AR069619, NIH/NIAMS K01-AR066743 (to XSL), NIH/NIAMS R01-AR071718 (to XSL), and NSF Graduate Research Fellowship (to CMJdB). We would like to thank Carlos Osuna for constructive criticism of the manuscript.

CONFLICT OF INTEREST

All authors have no conflict of interest.

REFERENCES

- Altman, A. R., W. J. Tseng, C. M. de Bakker, A. Chandra, S. Lan, B. K. Huh, S. Luo, M. Leonard, L. Qin, and X. S. Liu. Quantification of skeletal growth, modeling, and remodeling by *in vivo* micro computed tomography. *Bone* 81:370–379, 2015.
- Birkhold, A. I., H. Razi, G. N. Duda, R. Weinkamer, S. Checa, and B. M. Willie. The influence of age on adaptive bone formation and bone resorption. *Biomaterials* 35:9290–9301, 2014.
- Birkhold, A. I., H. Razi, G. N. Duda, R. Weinkamer, S. Checa, and B. M. Willie. Mineralizing surface is the main target of mechanical stimulation independent of age: 3D dynamic *in vivo* morphometry. *Bone* 66:15–25, 2014.
- Brouwers, J. E., B. van Rietbergen, and R. Huiskes. No effects of *in vivo* micro-CT radiation on structural parameters and bone marrow cells in proximal tibia of wistar rats detected after eight weekly scans. *J Orthop. Res.* 25:1325–1332, 2007.
- Campbell, G. M., H. R. Buie, and S. K. Boyd. Signs of irreversible architectural changes occur early in the development of experimental osteoporosis as assessed by *in vivo* micro-CT. *Osteoporos. Int.* 19(10):1409–1419, 2008.
- Campbell, G. M., and A. Sophocleous. Quantitative analysis of bone and soft tissue by micro-computed tomography: applications to *ex vivo* and *in vivo* studies. *Bonekey Rep.* 3:564, 2014.
- Cao, X., X. Wu, D. Frassica, B. Yu, L. Pang, L. Xian, M. Wan, W. Lei, M. Armour, E. Tryggstad, J. Wong, C. Y. Wen, W. W. Lu, and F. J. Frassica. Irradiation induces bone injury by damaging bone marrow microenvironment for stem cells. *Proc. Natl. Acad. Sci. U.S.A.* 108:1609–1614, 2011.
- Chandra, A., T. Lin, M. B. Tribble, J. Zhu, A. R. Altman, W. J. Tseng, Y. Zhang, S. O. Akintoye, K. Cengel, X. S. Liu, and L. Qin. PTH1-34 alleviates radiotherapy-induced local bone loss by improving osteoblast and osteocyte survival. *Bone* 67:33–40, 2014.
- Collignon, A., F. Maes, D. Delaere, D. Vandermeulen, P. Suetens, and G. Marchal. Automated multi-modality image registration based on information theory. In: *Information processing in medical imaging*, edited by Y. Bizais, C. Barillot, and R. Di Paola. Dordrecht: Kluwer, 1995, pp. 263–274.
- de Bakker, C. M., A. R. Altman, C. Li, M. B. Tribble, C. Lott, W. J. Tseng, and X. S. Liu. Minimizing interpolation bias and precision error in *in vivo* microCT-based measurements of bone structure and dynamics. *Ann. Biomed. Eng.* 44:2518–2528, 2016.
- Dudziak, M. E., P. B. Saadeh, B. J. Mehrara, D. S. Steinbrech, J. A. Greenwald, G. K. Gittes, and M. T. Longaker. The effects of ionizing radiation on osteoblast-like cells *in vitro*. *Plast. Reconstr. Surg.* 106:1049–1061, 2000.
- Gal, T. J., T. Munoz-Antonia, C. A. Muro-Cacho, and D. W. Klotch. Radiation effects on osteoblasts *in vitro*: a potential role in osteoradionecrosis. *Arch. Otolaryngol. Head Neck Surg.* 126:1124–1128, 2000.
- Glatt, V., E. Canalis, L. Stadmeier, and M. L. Bouxsein. Age-related changes in trabecular architecture differ in female and male C57BL/6J mice. *J. Bone Miner. Res.* 22:1197–1207, 2007.
- Klinck, R. J., G. M. Campbell, and S. K. Boyd. Radiation effects on bone architecture in mice and rats resulting from *in vivo* micro-computed tomography scanning. *Med. Eng. Phys.* 30:888–895, 2008.
- Kohler, T., M. Beyeler, D. Webster, and R. Muller. Compartmental bone morphometry in the mouse femur: reproducibility and resolution dependence of microtomographic measurements. *Calcif. Tissue Int.* 77:281–290, 2005.
- Kondo, H., N. D. Searby, R. Mojarrab, J. Phillips, J. Alwood, K. Yumoto, E. A. Almeida, C. L. Limoli, and R. K. Globus. Total-body irradiation of postpubertal mice with (137)Cs acutely compromises the microarchitecture of cancellous bone and increases osteoclasts. *Radiat. Res.* 171:283–289, 2009.
- Lambers, F. M., F. A. Schulte, G. Kuhn, D. J. Webster, and R. Muller. Mouse tail vertebrae adapt to cyclic mechanical loading by increasing bone formation rate and decreasing bone resorption rate as shown by time-lapsed *in vivo* imaging of dynamic bone morphometry. *Bone* 49:1340–1350, 2011.
- Lan, S., S. Luo, B. K. Huh, A. Chandra, A. R. Altman, L. Qin, and X. S. Liu. 3D image registration is critical to ensure accurate detection of longitudinal changes in trabecular bone density, microstructure, and stiffness measurements in rat tibiae by *in vivo* micro computed tomography (μ CT). *Bone* 56:83–90, 2013.
- Laperre, K., M. Depypere, N. van Gastel, S. Torrekens, K. Moermans, R. Bogaerts, F. Maes, and G. Carmeliet. Development of micro-CT protocols for *in vivo* follow-up of mouse bone architecture without major radiation side effects. *Bone* 49:613–622, 2011.
- Lu, Y., M. Boudiffa, E. Dall’Ara, I. Bellantuono, and M. Viceconti. Evaluation of *in vivo* measurement errors associated with micro-computed tomography scans by means of

- the bone surface distance approach. *Med. Eng. Phys.* 37:1091–1097, 2015.
- ²¹Lu, Y., M. Boudiffa, E. Dall'Ara, I. Bellantuono, and M. Viceconti. Development of a protocol to quantify local bone adaptation over space and time: quantification of reproducibility. *J. Biomech.* 49:2095–2099, 2016.
- ²²Matsumura, S., A. Jikko, H. Hiranuma, A. Deguchi, and H. Fuchihata. Effect of X-ray irradiation on proliferation and differentiation of osteoblast. *Calcif. Tissue Int.* 59:307–308, 1996.
- ²³Nishiyama, K. K., G. M. Campbell, R. J. Klinck, and S. K. Boyd. Reproducibility of bone micro-architecture measurements in rodents by in vivo micro-computed tomography is maximized with three-dimensional image registration. *Bone* 46:155–161, 2010.
- ²⁴Sawajiri, M., J. Mizoe, and K. Tanimoto. Changes in osteoclasts after irradiation with carbon ion particles. *Radiat. Environ. Biophys.* 42:219–223, 2003.
- ²⁵Schroeder, L. I. W., L. Ng, and J. Cates. *The ITK Software Guide*. The Insight Consortium. Cambridge: Cambridge University Press, 2003.
- ²⁶Schroeder, W., L. Ng, and J. Cates. *The ITK software guide second edition updated for ITK version 2.4*. *FEBS Lett.* 525:53–58, 2015.
- ²⁷Schulte, F. A., F. M. Lambers, G. Kuhn, and R. Muller. In vivo micro-computed tomography allows direct three-dimensional quantification of both bone formation and bone resorption parameters using time-lapsed imaging. *Bone* 48:433–442, 2011.
- ²⁸Schulte, F. A., F. M. Lambers, D. J. Webster, G. Kuhn, and R. Muller. In vivo validation of a computational bone adaptation model using open-loop control and time-lapsed micro-computed tomography. *Bone* 49:1166–1172, 2011.
- ²⁹Shrout, P. E., and J. L. Fleiss. Intraclass correlations: uses in assessing rater reliability. *Psychol. Bull.* 86:420–428, 1979.
- ³⁰Szymczyk, K. H., I. M. Shapiro, and C. S. Adams. Ionizing radiation sensitizes bone cells to apoptosis. *Bone* 34:148–156, 2004.
- ³¹Waarsing, J. H., J. S. Day, J. C. van der Linden, A. G. Ederveen, C. Spanjers, N. De Clerck, A. Sasov, J. A. Verhaar, and H. Weinans. Detecting and tracking local changes in the tibiae of individual rats: a novel method to analyse longitudinal in vivo micro-CT data. *Bone* 34:163–169, 2004.
- ³²Willey, J. S., S. A. Lloyd, M. E. Robbins, J. D. Bourland, H. Smith-Sielicki, L. C. Bowman, R. W. Norrdin, and T. A. Bateman. Early increase in osteoclast number in mice after whole-body irradiation with 2 Gy X rays. *Radiat Res.* 170:388–392, 2008.
- ³³Willie, B. M., A. I. Birkhold, H. Razi, T. Thiele, M. Aido, B. Kruck, A. Schill, S. Checa, R. P. Main, and G. N. Duda. Diminished response to in vivo mechanical loading in trabecular and not cortical bone in adulthood of female C57Bl/6 mice coincides with a reduction in deformation to load. *Bone* 55:335–346, 2013.

Publisher's Note Springer Nature remains neutral with regard to jurisdictional claims in published maps and institutional affiliations.